bioengineering

MDPI

Article

Reinvestigation of Absorption Spectroscopic Thermal Dynamics of Archaerhodopsin 3 Based Voltage Sensor Quasar1

Alfons Penzkofer [1,*], Arita Silapetere [2] and Peter Hegemann [2]

[1] Fakultät für Physik, Universität Regensburg, Universitätsstraße 31, D-93053 Regensburg, Germany
[2] Experimentelle Biophysik, Institut für Biologie, Humboldt Universität zu Berlin, Invalidenstraße 42, D-10115 Berlin, Germany
* Correspondence: alfons.penzkofer@physik.uni-regensburg.de; Tel.: +49-941-943-2107

Abstract

The long-time absorption spectroscopic development of the genetically encoded microbial rhodopsin fluorescent voltage indicator QuasAr1 at room temperature in the dark was reinvestigated, mainly theoretically. The data analysis indicates protein aggregation within one day to some ten-nanometer sized Mie scattering particles. The absorption coefficient spectra can be deduced from measured attenuation coefficient spectra by scattering contribution subtraction. The initially present protonated retinal Schiff base (PRSB) Ret_580 isomerized and then deprotonated to neutral retinal Schiff base (RSB). One part of Ret_580, Ret_580_I, (fraction 43%), isomerized moderately fast to Ret_500 which then deprotonated to neutral retinal Schiff base Ret_405 (time constant ≈ 1000 h). The other part of Ret_580, Ret_580_{II}, (fraction 57%), isomerized slowly to Ret_460 which deprotonated to Ret_340 (time constant ≈ 400 h). The dynamics are described by a differential equation system which is solved numerically. Reaction parameters are determined by fitting the simulations to the experimental results.

Keywords: QuasAr1; Archaerhodopsin; fluorescent voltage sensor; absorption spectroscopic characterization; protein aggregation; Rayleigh and Mie scattering; numerical simulation of thermal dynamics; ground-state isomerization; ground-state deprotonation

Academic Editor: Rossana Madrid

Received: 22 October 2025
Revised: 7 November 2025
Accepted: 18 November 2025
Published: 24 November 2025

Citation: Penzkofer, A.; Silapetere, A.; Hegemann, P. Reinvestigation of Absorption Spectroscopic Thermal Dynamics of Archaerhodopsin 3 Based Voltage Sensor Quasar1. *Bioengineering* **2025**, *12*, 1293. https://doi.org/10.3390/bioengineering12121293

1. Introduction

The protein QuasAr1 was derived from Archaerhodopsin 3 (Arch) of *Halorubrum sodomense* [1–3] by directed evolution [4] (QuasAr1 = Arch P60S-T80S-D106H-F161V). QuasAr1 is one member of a wide group of microbial rhodopsin-based fluorescent genetically encoded voltage indicators (GEVIs) [5–12] applied in optical electrophysiology of biological membrane potential determination [13,14]. QuasAr1 was used and characterized as a transmembrane voltage sensor in neuroscience [4,15] and cardiac science [16]. The thermal absorption and emission spectroscopic behavior of QuasAr1 was investigated in [17]. Here the long-time absorption development at room temperature in the dark was analyzed in detail and the model of thermal dynamics presented in [17] was modified. The temporal Rayleigh and Mie scattering evolution was studied. The absorption coefficient spectra development was extracted from measured attenuation coefficient spectra by subtracting scattering contributions. The absorption spectra development was determined by isomerization of the originally present protonated retinal Schiff base (PRSB) and deprotonation of the formed isomers to neutral retinal Schiff base (RSB). The isomerization and deprotonation dynamics were analyzed by a differential

equation system which was solved numerically. Reaction parameters were extracted by numerical fitting to experimental results.

The experimental attenuation coefficient spectra development, $\alpha(\lambda, t)$, at room temperature presented in ref. [17] (Figure S6) was redrawn (present Figure 1). The long-wavelength attenuation development (Figure 2), due to thermally driven protein aggregation, was analyzed, applying the Mie scattering theory. The absorption coefficient spectra development, $\alpha_a(\lambda, t)$, was deduced from the attenuation coefficient spectra development by empirical subtraction of the Mie scattering contribution, $\alpha_s(\lambda, t)$ (Figure 3). The initial absorption coefficient spectrum, originating from contributions of (i) protonated retinal Schiff base (PRSB) Ret_580 (absorption maximum at wavelength $\lambda = 580 \pm 2$ nm), (ii) residual retinals (weak absorption contribution below 450 nm) and (iii) apoprotein (peak absorption around 280 nm), evolved by Ret_580 degradation (ground-state thermal isomerization). The speed of Ret_580 isomerization changed with time (Figure S11): The fast component, Ret_580_I, built up a new absorption band peaking at $\lambda = 500 \pm 5$ nm (Ret_500), and the slow component, Ret_580_II, formed a weak absorption band at $\lambda = 460 \pm 10$ nm (Ret_460). The Ret_580 degradation spectra development is shown in Figure 4 by presenting the absorption coefficient difference spectra $\Delta\alpha_a(\lambda, t) = \alpha_a(\lambda, t) - \alpha_{a,\text{Ret\_580}}(\lambda, t) - \alpha_{a,\text{residual retinals}}(\lambda, 0) - \alpha_{a,\text{apoprotein}}(\lambda, 0)$. The initial $\Delta\alpha_a(\lambda, t)$ development is determined by Ret_500 formation. At longer times, the $\Delta\alpha_a(\lambda, t)$ development is determined by Ret_500 degradation (deprotonation to Ret_405 with absorption band peaking at $\lambda = 405 \pm 5$ nm) as well as Ret_460 formation and degradation (deprotonation to Ret_340 with the absorption band peaking at $\lambda = 340 \pm 15$ nm). The absorption coefficient double difference spectra $\Delta\Delta\alpha_a(\lambda, t) = \Delta\alpha_a(\lambda, t) - \alpha_{a,\text{Ret\_500}}(\lambda, t)$ (Figure 5) show the absorption coefficient development due to Ret_460 isomer formation, Ret_405 formation by Ret_500 deprotonation, and Ret_340 formation due to Ret_460 deprotonation. In the short-wavelength region, $\lambda < 300$ nm, apoprotein absorption increase is observed (Figures 3–5).

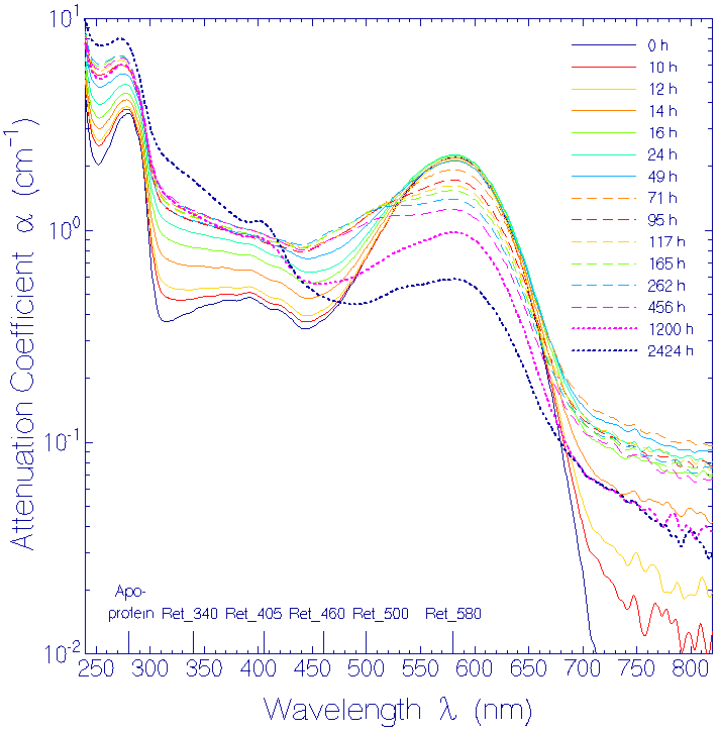

Figure 1. Temporal development of attenuation coefficient spectra $\alpha(\lambda)$ of QuasAr1 in pH 8 Tris buffer at room temperature (ϑ = 21–25 °C) in the dark. The storage times are listed in the legend.

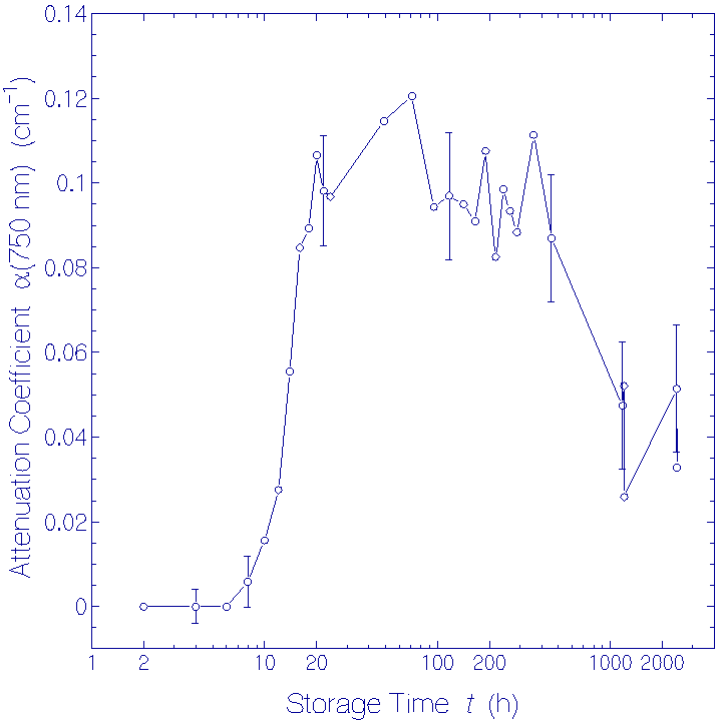

Figure 2. Attenuation coefficient α(750 nm) development versus storage time t at room temperature in the dark of QuasAr1 in pH 8 Tris buffer.

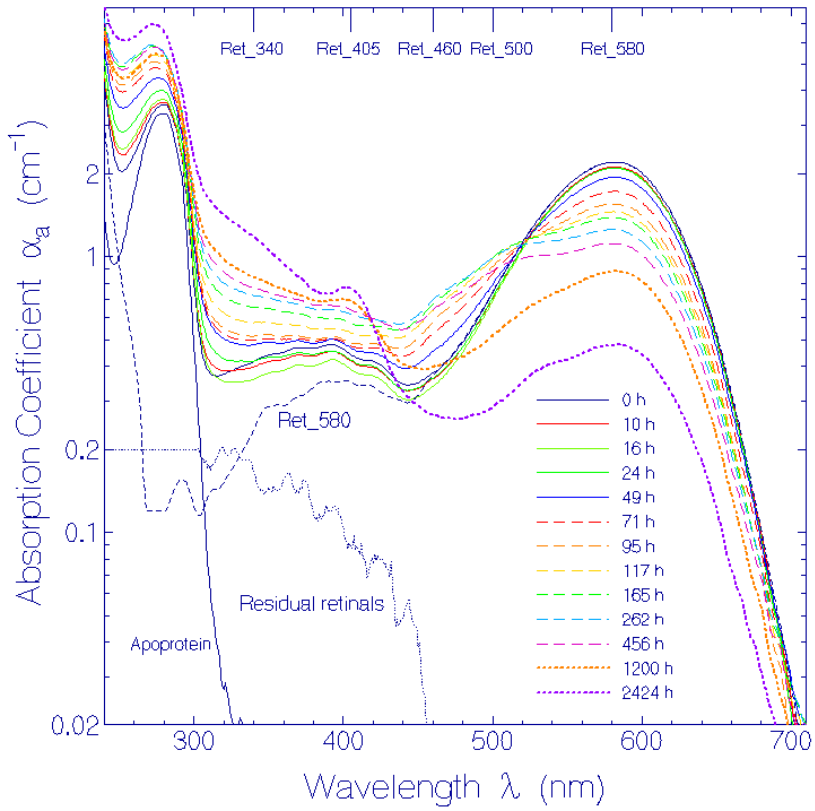

Figure 3. Determined absorption coefficient spectra α_a of QuasAr1 in pH 8 Tris buffer at room temperature in the dark. The storage time t is listed in the legend. The absorption coefficient spectra $\alpha_{a,\text{residual retinals}}(\lambda, t = 0)$, $\alpha_{a,\text{apoprotein}}(\lambda, t = 0)$, and $\alpha_{a,\text{Ret\_580}}(\lambda, t = 0) = \alpha_a(\lambda, t = 0) - \alpha_{a,\text{residual retinals}}(\lambda, t = 0) - \alpha_{a,\text{apoprotein}}(\lambda, t = 0)$ are included.

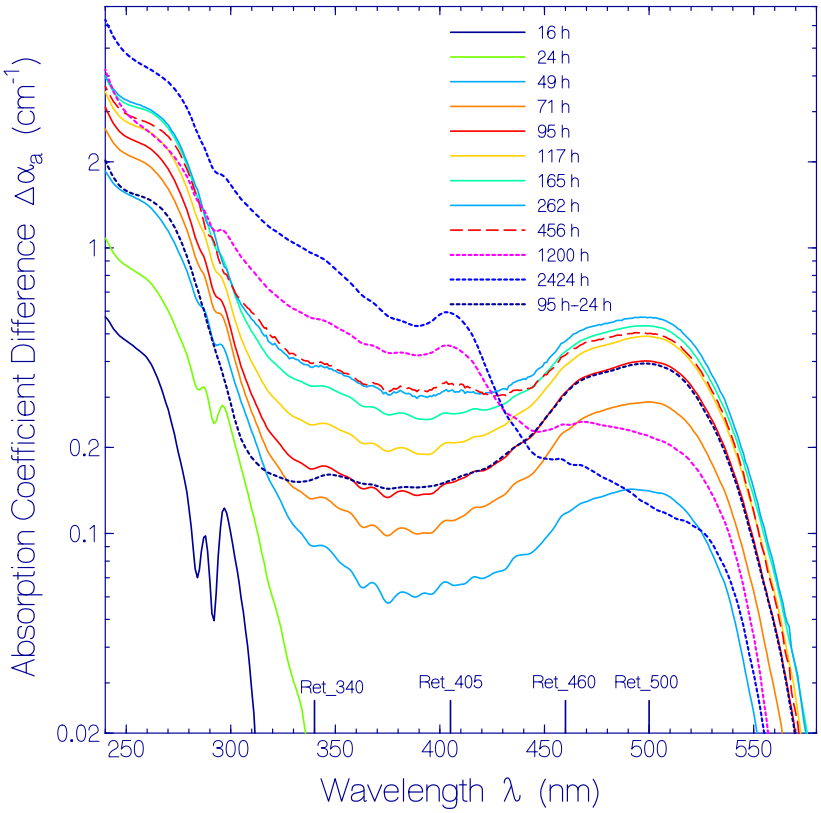

Figure 4. Temporal development of absorption of decomposition products of Ret_580: PRSB isomers Ret_500, Ret_460, and deprotonated RSB components Ret_405 and Ret_340. The absorption coefficient difference $\Delta\alpha_a(\lambda, t) = \alpha_a(\lambda, t) - \alpha_{\mathrm{a,Ret\_580}}(\lambda, t) - \alpha_{a,\text{residual retinals}}(\lambda, t = 0) - \alpha_{\mathrm{a,apoprotein}}(\lambda, t = 0)$ is displayed.

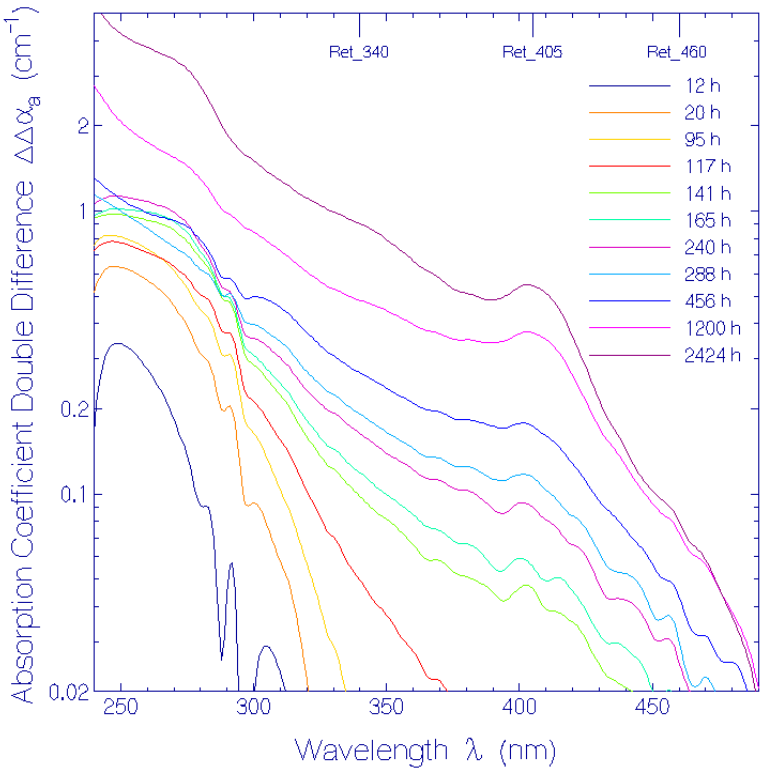

Figure 5. Temporal development of absorption of isomer product Ret_460, and deprotonation products Ret_405 and Ret_340. The absorption coefficient double difference $\Delta\Delta\alpha_a(\lambda, t) = \Delta\alpha_a(\lambda, t) - \alpha_{\mathrm{a,Ret\_500}}(\lambda, t)$ is displayed.

The isomerization and deprotonation dynamics was analyzed by a differential equation system which was solved numerically. Various absorption cross-sections, isomerization time constants, and deprotonation time constants were determined by simulating the temporal dependence of $\alpha_a(t)$ at 580 nm, $\Delta\alpha_a(t)$ at 500 nm, 460 nm, 405 nm, and 340 nm, and of $\Delta\Delta\alpha_a(t)$ at 460 nm, 405 nm, and 340 nm.

2. Materials and Methods

The QuasAr1 gene was a gift from Adam E. Cohen (Addgene plasmid # 64135, [4]). The sample preparation of QuasAr1 was reported in ref. [17]. The expressed QuasAr1 protein in the final buffer, containing 50 mM Tris-HCl (pH 8.0), 150 mM NaCl, 0.02% DDM, 0.004% CHS, 0.1 mM PMSF, and 5% glycerol, was aliquoted to amounts of 30 µL in Eppendorf tubes, shock-frozen, and stored at −80 °C until thawing for experimental investigations.

The transmission measurements, $T(\lambda) = \exp(-\alpha(\lambda)\ell)$, were carried out with a spectrophotometer (Cary 50, Varian Australia Pty Ltd., Mulgrave, Victoria, Australia) as described in ref. [17].

The thawed QuasAr1 solution was filled in a fused silica ultra-micro cell (inner cell size 1.5 × 3 × 5 mm^3, from Hellma Analytics, Müllheim, Germany). The cell length for the transmission measurements was ℓ = 3 mm. It was centrifuged with 4400 rpm for 30 min at 4 °C (Centrifuge 5702 R, Eppendorf AG, Hamburg, Germany). Then the sample was stored at room temperature (21–25 °C) in the dark and transmission spectra were measured at certain time intervals. After the absorption measurement at storage time t = 1200 h, the sample was centrifuged with 4400 rpm for 30 min at 4 °C, and then at t = 1201 h the absorption spectrum was measured again. After that, a fluorescence spectroscopic analysis occurred (see ref. [17]). Then, the sample was stored for further 51 days in the dark at room temperature before a further absorption measurement was carried out at t = 2424 h. Then the sample was centrifuged with 4400 rpm for 20 min at 4 °C. Finally, at t = 2425 h the last absorption spectrum measurement was carried out.

3. Results

3.1. Temporal Development of Attenuation Coefficient Spectra

The temporal development of attenuation coefficient spectra α(λ) of QuasAr1 in pH 8 Tris buffer at room temperature (ϑ = 21–25 °C) in the dark is presented in Figure S6 of ref. [17]. The spectra are redrawn in Figure 1 using a logarithmic attenuation coefficient ordinate (linear ordinate scale drawing is presented in Figure S1 of the Supplementary Materials). The long-wavelength part (λ > 710 nm) shows a significant rise of light attenuation between 10 h and 24 h, a leveling-off between 24 h and 456 h, and then some decrease in light attenuation. This attenuation behavior in the transparency region of QuasAr1 is due to Rayleigh scattering and Mie scattering caused by protein aggregation. With storage time, the attenuation decreased around 580 nm (PRSB, Ret_580), new attenuation built-up and decreased around 500 nm (PRSB, Ret_500) and 460 nm (PRSB, Ret_460), and it built-up around 405 nm (RSB, Ret_405) and 340 nm (RSB, Ret_340). Below 300 nm (apoprotein region) the attenuation rise is thought to be due to Mie scattering, formed retinal component absorption, and apoprotein absorption increase.

3.2. Mie Scattering Due to QuasAr1 Aggregation

The temporal attenuation coefficient development at λ = 750 nm in the spectral transparency region of QuasAr1 is displayed in Figure 2. Within the first 6 h no attenuation was observed. In the time range between 10 h and 24 h the light attenuation rose steeply to

$\alpha = 0.105 \pm 0.015\ cm^{-1}$, then it kept approximately constant within the next 15 days, and eventually decreased to $\alpha = 0.05 \pm 0.015\ cm^{-1}$ at a storage time of $t = 101$ d.

The light attenuation coefficient $\alpha(\lambda)$ in the transparency region is equal to the light scattering coefficient $\alpha_s(\lambda)$. The light scattering is thought to be due to QuasAr1 aggregation. For small aggregate size, diameter $d < 0.05\ \lambda/n_w$ where n_w is the refractive index of the solvent (here water), the Rayleigh scattering theory is responsible [18–21]. For larger aggregate size the Mie scattering theory is appropriate [18,19,21–25].

From the scattering coefficient dependence displayed in Figure 2, the QuasAr1 aggregation behavior is analyzed in Section S2 of the Supplementary Materials. There, the monomeric Rayleigh scattering cross-section, $\sigma_{R,m}(750\ nm) \approx 5 \times 10^{-22}\ cm^2$, the aggregation scattering enhancement factor development, $M_{sca}(t)$, the degree of aggregation development, $\beta_m(t)$, and the refractive index of QuasAr1, $n_Q(750\ nm) \approx 1.6029$, are determined.

3.3. Absorption Coefficient Development

The temporal absorption coefficient development $\alpha_a(\lambda, t)$ was determined from the measured attenuation coefficient development $\alpha(\lambda, t)$ presented in Figure 1 by subtracting the scattering contribution $\alpha_s(\lambda, t)$ according to $\alpha_a(\lambda, t) = \alpha(\lambda, t) - \alpha_s(\lambda, t)$. The scattering contribution was calculated by the empirical relation $\alpha_s(\lambda, t) = \alpha_s(\lambda_0, t) \times (\lambda_0/\lambda)^{\gamma(t)}$ with a reference wavelength λ_0 in the transparency region and the Mie scattering power factor $\gamma < 4$ [26,27]. The reference wavelength was set to $\lambda_0 = 900$ nm. The Mie scattering power factor γ was adjusted to the strength of light scattering by trial and error. The applied scattering coefficient spectra, $\alpha_s(\lambda, t)$, are shown in Figure S8, and the thereby used power factor dependence, $\gamma(t)$, is shown in Figure S9 of the Supplementary Materials. The accuracy of $\alpha_s(\lambda)$ determination reduced with decreasing wavelength because of inverse potential wavelength dependence and direct scattering observation only in the transparency region.

The obtained absorption coefficient spectra $\alpha_a(\lambda, t)$ are displayed in Figure 3 with logarithmic ordinate scale (linear representation in Figure S2 of the Supplementary Materials). The initial absorption coefficient spectrum, $\alpha_a(\lambda, t = 0)$ was composed of the absorption coefficient spectrum of the initially present protonated retinal Schiff base Ret_580, some residual retinals, and the apoprotein [17], i.e., $\alpha_a(\lambda, t = 0) = \alpha_{a,\text{Ret\_580}}(\lambda, t = 0) + \alpha_{a,\text{residual retinals}}(\lambda, t = 0) + \alpha_{\text{apoprotein}}(\lambda, t = 0)$. As already discussed for the attenuation spectra in Figure 1, with storage time t Ret_580 thermally isomerized to Ret_500 and Ret_460, and these protonated retinal Schiff bases deprotonated to Ret_405 and Ret_340 neutral retinal Schiff bases.

The absorption coefficient development at 580 nm, 500 nm, 460 nm, 405 nm, and 340 nm is displayed in Figure S3 of the Supplementary Materials. At 580 nm, which is the wavelength of peak Ret_580 absorption, the absorption initially decreased fast and then decreased slowly. Ret_580 indicates a two-component decay: one component, Ret_580_I, isomerized fast to Ret_500, showing a fast absorption increase at 500 nm, the other component, Ret_580_II, isomerized slowly to Ret_460. The absorption development at 500 nm, 460 nm, 405 nm, and 340 nm was caused by the isomerization of Ret_580_I to Ret_500 and of Ret_580_II to Ret_460 followed by deprotonation of Ret_500 to Ret_405 and of Ret_460 to Ret_340 (see below).

In order to better see the isomerization of Ret_580 to Ret_500 and Ret_460 as well as the deprotonation of Ret_500 to Ret_405 and of Ret_460 to Ret_340, absorption coefficient difference spectra, $\Delta\alpha_a(\lambda, t) = \alpha_a(\lambda, t) - \alpha_{a,\text{Ret\_580}}(\lambda, t) - \alpha_{a,\text{residual retinals}}(\lambda, t = 0) - \alpha_{a,\text{apoprotein}}(\lambda, t = 0)$, are displayed in Figure 4 (linear ordinate scale presentation in Figure S4 of the Supplementary Materials). In the storage time range $t < 117$ h the difference absorption spectra development is dominated by Ret_500 formation with absorption

peak at λ ≈ 500 nm. In the storage time range up to 456 h, Ret_500 formation levels off and Ret_460 formation at 460 nm gains importance. For longer storage times the absorption around 500 nm and 460 nm decreased and the absorption around 405 nm (Ret_405) and 340 nm (Ret_340) increased due to deprotonation of Ret_500 to Ret_405 and of Ret_460 to Ret_340. In Figure 4 the curve labeled '95 h–24 h' belonging to $\Delta\alpha_a(\lambda, 95\,\mathrm{h}) - \Delta\alpha_a(\lambda, 24\,\mathrm{h})$ resembles the shape of the absorption coefficient spectrum of Ret_500 for λ > 300 nm, because in this time range only the formation of Ret_500 is significant.

The absorption coefficient development of Ret_460, Ret_405 and Ret_340 is displayed in Figure 5 (linear ordinate scale presentation in Figure S5 of the Supplementary Materials) where absorption coefficient double difference spectra, $\Delta\Delta\alpha_a(\lambda, t) = \Delta\alpha_a(\lambda, t) - \alpha_{a,\mathrm{Ret\_500}}(\lambda, t)$ are shown for different storage times listed in the legend. The absorption coefficient growth around 460 nm (Ret_460 absorption) is moderate, since Ret_580 ($\mathrm{Ret\_580_{II}}$) isomerized slowly to Ret_460 and during its formation it deprotonated to Ret_340 showing up in the absorption around 340 nm. The absorption peaking around 405 nm was due to deprotonation of Ret_500 to Ret_405.

In Figure 6 the temporal development of the absorption coefficient, $\alpha_a(580\mathrm{nm}, t)$, and the absorption coefficient differences, $\Delta\alpha_a(500\ \mathrm{nm}, t)$, $\Delta\alpha_a(460\ \mathrm{nm}, t)$, $\Delta\alpha_a(405\ \mathrm{nm}, t)$, and $\Delta\alpha_a(340\ \mathrm{nm}, t)$, are displayed. The symbols are experimental results from Figures 3 and 4, and the curves are theoretical simulations (see below).

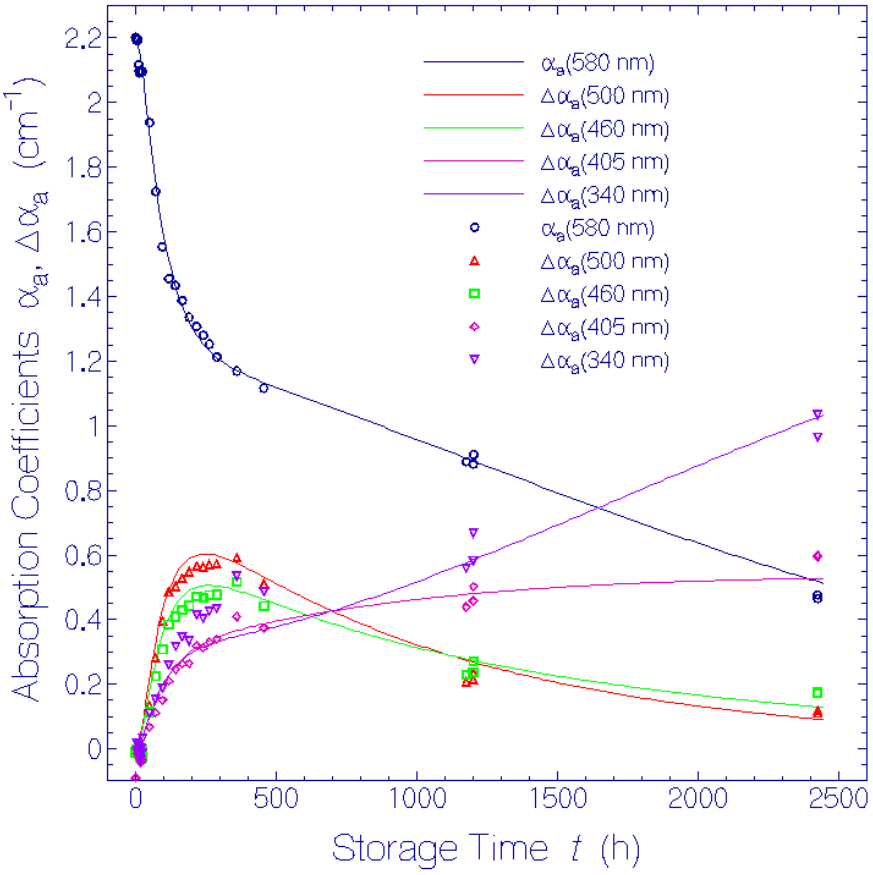

Figure 6. Temporal development of absorption coefficient α_a(580 nm) and of absorption coefficient differences $\Delta\alpha_a$ at specific wavelengths 500 nm, 460 nm, 405 nm and 340 nm for QuasAr1 in pH 8 Tris buffer during storage in the dark at room temperature. Points are experimental results. Curves are simulations.

The absorption coefficient development α_a(580 nm, t) indicates the fast ismerization of $\mathrm{Ret\_580_I}$ to Ret_500 and the slow isomerization of $\mathrm{Ret\_580_{II}}$ to Ret_460. The initial rise of

the absorption coefficient difference $\Delta\alpha_a$(500 nm, t) is due to Ret_500 formation because of isomerization of Ret_580$_I$, and the following decrease is due to Ret_500 deprotonation to Ret_405. The temporal dependence of $\Delta\alpha_a$(460 nm, t) is determined by the absorption behavior of Ret_500 and the absorption contribution of Ret_460 which is formed by isomerization of Ret_580$_{II}$ to Ret_460 and depleated by subsequent deprotonation of Ret_460 to Ret_340. $\Delta\alpha_a$(405 nm, t) is determined by absorption contributions of Ret_500, Ret_460, and the Ret_405 formation by deprotonation of Ret_500. $\Delta\alpha_a$(340 nm, t) is determined by absorption contributions of Ret_500, Ret_460, Ret_405, and the Ret_340 formation by deprotonation of Ret_460.

In Figure 7 the temporal development of the absorption coefficient double differences, $\Delta\Delta\alpha_a(460\text{ nm}, t)$, $\Delta\Delta\alpha_a(405\text{ nm}, t)$, and $\Delta\Delta\alpha_a(340\text{ nm}, t)$, are displayed. The symbols are experimental results from Figure 5 and the curves are theoretical simulations (see below).

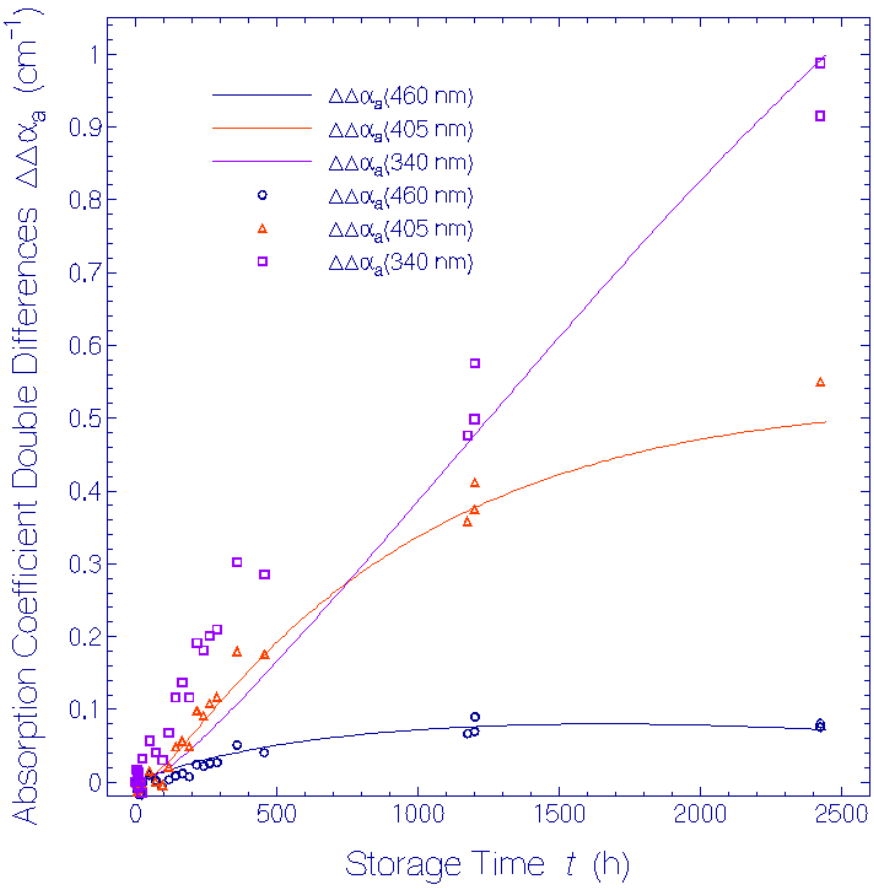

Figure 7. Temporal development of absorption coefficient double differences, $\Delta\Delta\alpha_a$ at specific wavelengths 460 nm, 405 nm, and 340 nm for QuasAr1 in pH 8 Tris buffer during storage in the dark at room temperature. Points are experimental results. Curves are simulations.

The absorption coefficient double difference dependence at 460 nm is equal to the absorption coefficient dependence of Ret_460, i.e., $\Delta\Delta\alpha_a(460\text{ nm}, t) = \alpha_{a,\text{Ret\_460}}(460\text{ nm}, t)$. The absorption coefficient double difference $\Delta\Delta\alpha_a$(405 nm, t) is given by $\Delta\Delta\alpha_a(405\text{ nm}, t) = \alpha_{a,\text{Ret\_460}}(405\text{ nm}, t) + \alpha_{a,\text{Ret\_405}}(405\text{ nm}, t)$. The absorption coefficient double difference $\Delta\Delta\alpha_a$(340 nm, t) is given by the sum of the absorption coefficients of Ret_460, $\alpha_{a,\text{Ret\_460}}(340\text{ nm}, t)$, Ret_405, $\alpha_{a,\text{Ret\_405}}(340\text{ nm}, t)$, Ret_340, $\alpha_{a,\text{Ret\_340}}(340\text{ nm}, t)$, and other decay products, $\alpha_{a,\text{other decay products}}(340\text{ nm}, t)$.

4. Theoretical Thermal Absorption Dynamics Simulation of QuasAr1

4.1. Scheme of QuasAr1 Isomerization and Deprotonation

The dominant temporal absorption development of QuasAr1 in pH 8 Tris buffer at room temperature in the dark is modeled by the scheme of Figure 8. The originally present protonated retinal Schiff base (PRSB) Ret_580 (likely *all-trans* conformation) is composed of two differently ground-state isomerizing fractions Ret_580_I and Ret_580_{II} probably due to different adjacent amino acid arrangement of the apoprotein around the retinal Schiff base cofactor. Ret_580_I isomerizes moderately fast to Ret_500 (likely 13-*cis* conformation in $apoprotein_I$ environment), and Ret_580_{II} isomerizes slowly to Ret_460 (likely 13-*cis* conformation in $apoprotein_{II}$ environment). Ret_500 deprotonates to the neutral retinal Schiff base (RSB) Ret_405, while Ret_460 deprotonates to RSB Ret_340.

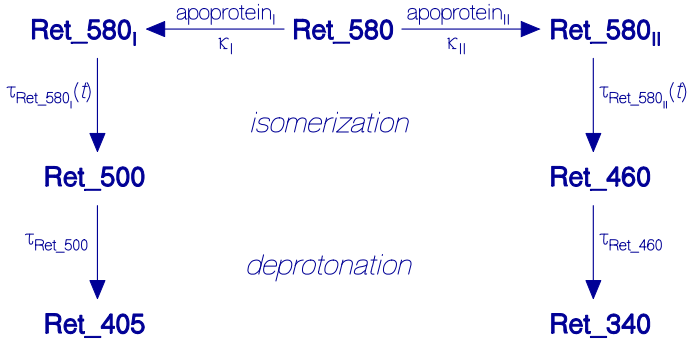

Figure 8. Scheme of dominant temporal dynamics of degradation of QuasAr1 in pH 8 Tris buffer in the dark at room temperature.

4.2. Numerical Simulation of QuasAr1 Thermal Dynamics

The experimental development of the protonated retinal Schiff base isomerization and subsquent deprotonation at room temperature in the dark is simulated numerically with a Fortran program using the following differential equation system for the number densities N_i of the populations in the retinal Schiff base constitutions of Figure 8.

The differential equation system for the temporal development of the level population number densities of the retinal components of Figure 8 reads (parameters are described in the symbols table at the end of the paper):

$$\frac{dN_{Ret\_580_I}}{dt} = -\frac{N_{Ret\_580_I}}{\tau_{Ret\_580_I}(t)}, \tag{1}$$

$$\frac{dN_{Ret\_580_{II}}}{dt} = -\frac{N_{Ret\_580_{II}}}{\tau_{Ret\_580_{II}}(t)}, \tag{2}$$

$$\frac{dN_{Ret\_500}}{dt} = \frac{N_{Ret\_580_I}}{\tau_{Ret\_580_I}(t)} - \frac{N_{Ret\_500}}{\tau_{Ret\_500}}, \tag{3}$$

$$\frac{dN_{Ret\_460}}{dt} = \frac{N_{Ret\_580_{II}}}{\tau_{Ret\_580_{II}}(t)} - \frac{N_{Ret\_460}}{\tau_{Ret\_460}}, \tag{4}$$

$$\frac{dN_{Ret\_405}}{dt} = \frac{N_{Ret\_500}}{\tau_{Ret\_500}}, \tag{5}$$

$$\frac{dN_{Ret\_340}}{dt} = \frac{N_{Ret\_460}}{\tau_{Ret\_460}}, \tag{6}$$

with approximate isomerization time constants

$$\tau_{\text{Ret\_580}_\text{I}}(t) = \left(\tau^0_{\text{Ret\_580}_\text{I}} - \tau^\infty_{\text{Ret\_580}_\text{I}}\right) \exp\left(-\frac{t}{\delta\tau_{\text{Ret\_580}_\text{I}}}\right) + \tau^\infty_{\text{Ret\_580}_\text{I}}, \tag{7}$$

$$\tau_{\text{Ret\_580}_\text{II}}(t) = \left(\tau^0_{\text{Ret\_580}_\text{II}} - \tau^\infty_{\text{Ret\_580}_\text{II}}\right) \exp\left(-\frac{t}{\delta\tau_{\text{Ret\_580}_\text{II}}}\right) + \tau^\infty_{\text{Ret\_580}_\text{II}}, \tag{8}$$

The intial conditions are:

$$N_{\text{Ret\_580}}(t=0) = N_{\text{Ret\_580,0}} = \alpha_a(\lambda = 580\text{ nm}, t=0)/\sigma_{a,\text{Ret\_580}}(\lambda = 580\text{ nm}), \tag{9}$$

$$N_{\text{Ret\_580}_\text{I}}(t=0) = \kappa_\text{I} N_{\text{Ret\_580}}(t=0), \tag{10}$$

$$N_{\text{Ret\_580}_\text{II}}(t=0) = \kappa_\text{II} N_{\text{Ret\_580}}(t=0), \tag{11}$$

$$N_{\text{Ret\_500}}(t=0) = 0, \tag{12}$$

$$N_{\text{Ret\_460}}(t=0) = 0, \tag{13}$$

$$N_{\text{Ret\_405}}(t=0) = 0, \tag{14}$$

$$N_{\text{Ret\_340}}(t=0) = 0. \tag{15}$$

$N_{\text{Ret\_580}}(t=0) = N_{\text{Ret\_580,0}} = 1.381 \times 10^{-16}$ cm^{-3} is determined using absorption coefficient $\alpha_a(\lambda = 580\text{ nm}, t=0) = 2.20$ cm^{-1} (Figure 3) and absorption cross-section $\sigma_{a,\text{Ret\_580}}(\lambda = 580\text{ nm}) = 1.593 \times 10^{-16}$ cm^2 (Figure S3 of [17] and Figure S10 of Supplementary Materials).

The unknown parameters are: κ_I, the initial fraction of Ret_580$_\text{I}$ in Ret_580; κ_II, the initial fraction of Ret_580$_\text{II}$ in Ret_580; $\tau^0_{\text{Ret\_580}_\text{I}}$, the initial time constant of Ret_580$_\text{I}$ isomerization; $\tau^\infty_{\text{Ret\_580}_\text{I}}$, the final time constant of Ret_580$_\text{I}$ isomerization; $\delta\tau_{\text{Ret\_580}_\text{I}}$, the exponential time constant of change-over from initial to final Ret_580$_\text{I}$ isomerization; $\tau^0_{\text{Ret\_580}_\text{II}}$, the initial time constant of Ret_580$_\text{II}$ isomerization; $\tau^\infty_{\text{Ret\_580}_\text{II}}$, the final time constant of Ret_580$_\text{II}$ isomerization; $\delta\tau_{\text{Ret\_580}_\text{II}}$, the exponential time constant of change-over from initial to final Ret_580$_\text{II}$ isomerization; $\tau_{\text{Ret\_500}}$, the time constant of Ret_500 deprotonation; and $\tau_{\text{Ret\_460}}$, the time constant of Ret_460 deprotonation.

The unknown parameters are determined by numerical fitting the experimental storage time development of the absorption coefficients $\alpha_a(\lambda = 580\text{ nm}, t)$, the absorption coefficient differences $\Delta\alpha_a(\lambda = 500\text{ nm}, t)$, $\Delta\alpha_a(\lambda = 460\text{ nm}, t)$, $\Delta\alpha_a(\lambda = 405\text{ nm}, t)$, $\Delta\alpha_a(\lambda = 340\text{ nm}, t)$, and the absorption coefficient double differences $\Delta\Delta\alpha_a(\lambda = 460\text{ nm}, t)$, $\Delta\Delta\alpha_a(\lambda = 405\text{ nm}, t)$, and $\Delta\Delta\alpha_a(\lambda = 340\text{ nm}, t)$.

The absorption coefficent developments are given by

$$\alpha_a(\lambda = 580\text{ nm}, t) = \left(N_{\text{Ret\_580}_\text{I}}(t) + N_{\text{Ret\_580}_\text{II}}(t)\right)\sigma_{a,\text{Ret\_580}}(\lambda = 580\text{ nm}), \tag{16}$$

$$\Delta\alpha_a(\lambda = 500\text{ nm}, t) = N_{\text{Ret\_500}}(t)\sigma_{a,\text{Ret\_500}}(\lambda = 500\text{ nm}) + N_{\text{Ret\_460}}(t)\sigma_{a,\text{Ret\_460}}(\lambda = 500\text{ nm}), \tag{17}$$

$$\begin{aligned}\Delta\alpha_a(\lambda = 460\text{ nm}, t) = {} & N_{\text{Ret\_500}}(t)\sigma_{a,\text{Ret\_500}}(\lambda = 460\text{ nm}) + N_{\text{Ret\_460}}(t)\sigma_{a,\text{Ret\_460}}(\lambda = 460\text{ nm}) \\ & + N_{\text{Ret\_405}}(t)\sigma_{a,\text{Ret\_405}}(\lambda = 460\text{ nm})\end{aligned}, \tag{18}$$

$$\begin{aligned}\Delta\alpha_a(\lambda = 405\text{ nm}, t) = {} & N_{\text{Ret\_500}}(t)\sigma_{a,\text{Ret\_500}}(\lambda = 405\text{ nm}) + N_{\text{Ret\_460}}(t)\sigma_{a,\text{Ret\_460}}(\lambda = 405\text{ nm}) \\ & + N_{\text{Ret\_405}}(t)\sigma_{a,\text{Ret\_405}}(\lambda = 405\text{ nm})\end{aligned}, \tag{19}$$

$$\begin{aligned}\Delta\alpha_a(\lambda = 340\text{ nm}, t) = {} & N_{\text{Ret\_500}}(t)\sigma_{a,\text{Ret\_500}}(\lambda = 340\text{ nm}) + N_{\text{Ret\_460}}(t)\sigma_{a,\text{Ret\_460}}(\lambda = 340\text{ nm}) \\ & + N_{\text{Ret\_405}}(t)\sigma_{a,\text{Ret\_405}}(\lambda = 340\text{ nm}) + N_{\text{Ret\_340}}(t)\sigma_{a,\text{Ret\_340}}(\lambda = 340\text{ nm})\end{aligned}, \tag{20}$$

$$\Delta\Delta\alpha_a(\lambda = 460\ \text{nm}, t) = \begin{matrix} N_{\text{Ret\_460}}(t)\sigma_{a,\text{Ret\_460}}(\lambda = 460\ \text{nm}) \\ +N_{\text{Ret\_405}}(t)\sigma_{a,\text{Ret\_405}}(\lambda = 460\ \text{nm}) \end{matrix}, \quad (21)$$

$$\Delta\Delta\alpha_a(\lambda = 405\ \text{nm}, t) = \begin{matrix} N_{\text{Ret\_460}}(t)\sigma_{a,\text{Ret\_460}}(\lambda = 405\ \text{nm}) \\ +N_{\text{Ret\_405}}(t)\sigma_{a,\text{Ret\_405}}(\lambda = 405\ \text{nm}) \end{matrix}, \quad (22)$$

$$\begin{matrix} \Delta\Delta\alpha_a(\lambda = 340\ \text{nm}, t) = N_{\text{Ret\_460}}(t)\sigma_{a,\text{Ret\_460}}(\lambda = 340\ \text{nm}) \\ +N_{\text{Ret\_405}}(t)\sigma_{a,\text{Ret\_405}}(\lambda = 340\ \text{nm}) + N_{\text{Ret\_340}}(t)\sigma_{a,\text{Ret\_340}}(\lambda = 340\ \text{nm}) \end{matrix} \quad (23)$$

The simulated curves, $\alpha_a(\lambda = 580\ \text{nm}, t)$, $\Delta\alpha_a(\lambda = 500\ \text{nm}, t)$, $\Delta\alpha_a(\lambda = 460\ \text{nm}, t)$, $\Delta\alpha_a(\lambda = 405\ \text{nm}, t)$, and $\Delta\alpha_a(\lambda = 340\ \text{nm}, t)$ are shown in Figure 6, and the simulated curves, $\Delta\Delta\alpha_a(\lambda = 460\ \text{nm}, t)$, $\Delta\Delta\alpha_a(\lambda = 405\ \text{nm}, t)$, and $\Delta\Delta\alpha_a(\lambda = 340\ \text{nm}, t)$ are shown in Figure 7. The applied parameters in the simulations are collected in Table 1. The ±-digits indicate uncertainties of the values.

Table 1. Parameters for QuasAr1 in pH 8 Tris buffer at room temperature in the dark.

Parameter	Value	Comment
κ_I	0.43 ± 0.02	In Equation (10)
κ_{II}	0.57 ± 0.02	In Equation (11)
$\tau^0_{\text{Ret\_580}_I}$	450 ± 50 h	In Equation (7)
$\tau^\infty_{\text{Ret\_580}_I}$	80 ± 10 h	In Equation (7)
$\delta\tau_{\text{Ret\_580}_I}$	13 ± 1 h	In Equation (7)
$\tau^0_{\text{Ret\_580}_{II}}$	5000 ± 300 h	In Equation (8)
$\tau^\infty_{\text{Ret\_580}_{II}}$	1700 ± 100 h	In Equation (8)
$\delta\tau_{\text{Ret\_580}_{II}}$	1000 ± 50 h	In Equation (8)
$\tau_{\text{Ret\_500}}$	1000 ± 50 h	In Equation (3)
$\tau_{\text{Ret\_460}}$	400 ± 30 h	In Equation (4)
$\sigma_{\text{Ret\_580}}(580\ \text{nm})$	$(1.593 \pm 0.05) \times 10^{-16}\ \text{cm}^2$	See Figure S10, and [17]
$\sigma_{\text{Ret\_500}}(500\ \text{nm})$	$(1.25 \pm 0.05) \times 10^{-16}\ \text{cm}^2$	See Figure S10
$\sigma_{\text{Ret\_500}}(460\ \text{nm})$	$(1.0 \pm 0.05) \times 10^{-16}\ \text{cm}^2$	See Figure S10
$\sigma_{\text{Ret\_500}}(405\ \text{nm})$	$(5.47 \pm 0.05) \times 10^{-17}\ \text{cm}^2$	See Figure S10
$\sigma_{\text{Ret\_500}}(340\ \text{nm})$	$(5.85 \pm 0.1) \times 10^{-17}\ \text{cm}^2$	See Figure S10
$\sigma_{\text{Ret\_460}}(500\ \text{nm})$	$(2.64 \pm 0.05) \times 10^{-17}\ \text{cm}^2$	See Figure S10
$\sigma_{\text{Ret\_460}}(460\ \text{nm})$	$(1.0 \pm 0.05) \times 10^{-16}\ \text{cm}^2$	See Figure S10
$\sigma_{\text{Ret\_460}}(405\ \text{nm})$	$(5.34 \pm 0.1) \times 10^{-17}\ \text{cm}^2$	See Figure S10
$\sigma_{\text{Ret\_460}}(340\ \text{nm})$	$(4.40 \pm 0.2) \times 10^{-17}\ \text{cm}^2$	See Figure S10
$\sigma_{\text{Ret\_405}}(460\ \text{nm})$	$(1.60 \pm 0.1) \times 10^{-18}\ \text{cm}^2$	See Figure S10
$\sigma_{\text{Ret\_405}}(405\ \text{nm})$	$(8.5 \pm 0.5) \times 10^{-17}\ \text{cm}^2$	See Figure S10
$\sigma_{\text{Ret\_405}}(340\ \text{nm})$	$(3.72 \pm 0.5) \times 10^{-17}\ \text{cm}^2$	See Figure S10
$\sigma_{\text{Ret\_340}}(340\ \text{nm})$	$(1.8 \pm 0.3) \times 10^{-16}\ \text{cm}^2$	In Equation (23)
$N_{\text{Ret\_580,0}}$	$(1.381 \pm 0.05) \times 10^{16}\ \text{cm}^{-3}$	In Equation (9)

The calculated normalized population number density development $N_i/N_{\text{Ret\_580,0}}$ versus storage time t is displayed in Figure 9. Thereby i stands for Ret_580_I, Ret_580_{II}, Ret_500, Ret_460, Ret_405, and Ret_340. $N_{\text{Ret\_580,0}}$ stands for the initial Ret_580 number density at $t = 0$. The number density of Ret_580_I decreases fast and causes the fast rise in the number density of Ret_500. Ret_500 decays slowly to Ret_405. Ret_580_{II} decreases slowly and causes the formation of Ret_460. The number density of Ret_460 remains small since Ret_460 decays with faster time constant to Ret_340 than it is formed. Ret 405 and Ret_340 continously grow up.

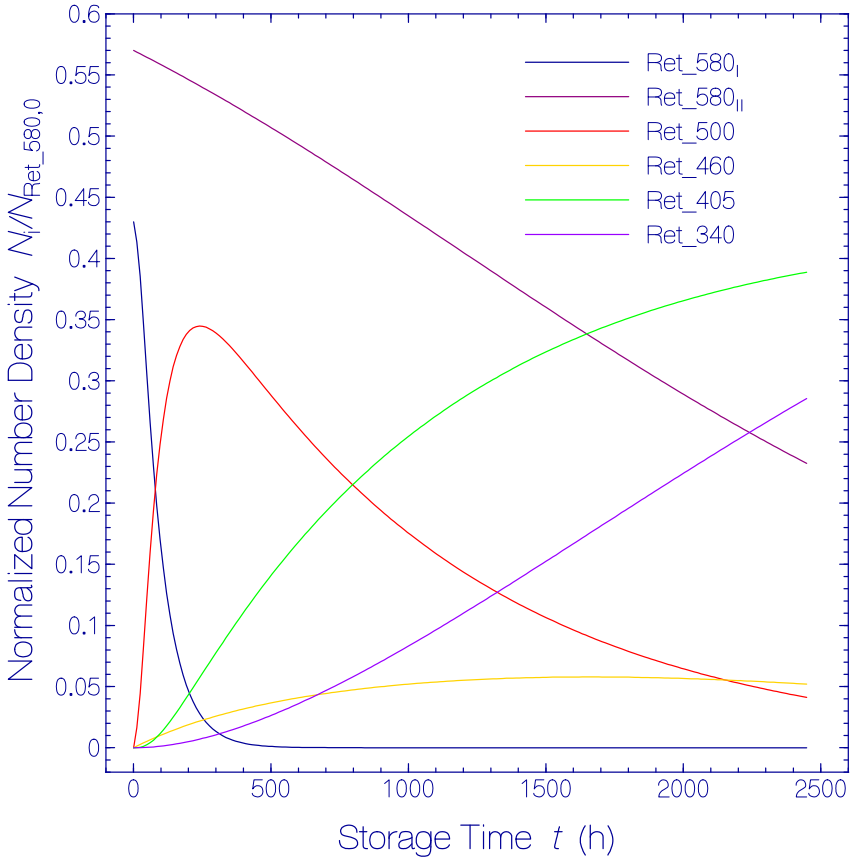

Figure 9. Temporal normalized population number density development, $N_i(t)N_{Ret\_580,0}$, of QuasAr1 constituents i = Ret_580$_I$, Ret_580$_{II}$, Ret_500, Ret_460, Ret_405, and Ret_340. $N_{Ret\_580,0} = N_{Ret\_580}$ (t = 0).

5. Discussion

The room temperature dynamics of the Archaerhodopsin 3 based fluorescent voltage sensor QuasAr1 studied in [17] has been reinvestigated, applying improved light scattering contibution subtraction and numerical simulation of the absorption development. The previously proposed dynamics of Ret_580$_{II}$ isomerization to Ret_640 (absorption peak at 640 nm) with fast Ret_640 deprotonation to Ret_350 could not be simulated. Refined scattering contribution subtraction led to the disappearance of the absorption coefficient difference $\Delta\alpha_a(t)$ around 640 nm shown in Figure 7b of ref. [17] (see new Figure S4 in the Supplementary Materials).

The attenuation coefficient development at λ = 750 nm depicted in Figure 2 indicates the onset of light scattering after a storage time of 6 h approaching a scattering plateau within about 24 h. This attenuation coefficient development is interpreted in Section S2 of the Supplementary Materials as QuasAr1 aggregation, and Rayleigh scattering and Mie scattering theory was applied there to gain information on the aggregation dynamics. The degree of aggegation approached $\beta_m \geq 14{,}000$, and aggregate particle radius $a_{ag} \geq 46$ nm. The QuasAr1 protein refractive index was calculated to be $n_Q = 1.6029$.

The absorption coefficient spectra development, $\alpha_a(\lambda, t)$, is shown in Figure 3, where the scattering contibution to the attenuation coeffcient spectra was subtracted, applying an empirical scattering coefficient spectra formula (Section S2.3 and Equation (S12) of the Supplementary Materials). To visualize the Ret_580 isomerization dynamics, the absorption coefficient difference spectra, $\Delta\alpha_a(\lambda, t)$, were calculated subtracting the Ret_580 contributions (Figure 4). The buildup of the isomer Ret_500 by Ret_580$_I$ isomerization within the first 300 h and its later decay due to deprotonation of Ret_500 to Ret_405 is

clearly seen. In Figure 5 the absorption coefficient double difference spectra, $\Delta\Delta\alpha_a(\lambda, t)$, are shown, obtained by subtracting the Ret_500 absorption coeffcient contributions. They reveal the formation of a weak absorption band around λ = 460 nm due to isomerization of Ret_580_{II} to Ret_460. Around λ = 405 nm the buildup of Ret_405 as a deprotonation product of Ret_500 can be seen clearly. The absorption band around λ = 340 nm is due to fast deprotonation of Ret_460 to Ret_340. The absorption rise below λ = 300 nm is dominantly attributed to inceasing apoprotein absorption due to apoprotein modification with storage time.

In Figure 6 the α_a(580 nm, *t*) dependence clearly shows the two-component degradation of Ret_580 (fast isomerization of Ret_580_I to Ret_500, and slow isomerization of Ret_580_{II} to Ret_460). The $\Delta\alpha_a$(500 nm, *t*) and $\Delta\alpha_a$(460 nm, *t*) dependences show the Ret_500 and Ret_460 buildups and decays. The $\Delta\alpha_a$(405 nm, *t*) and $\Delta\alpha_a$(340 nm, *t*) curves indicate the formation of the neutral retinal Schiff bases Ret_405 and Ret_340 due to deprotonation of Ret_500 and Ret_460, respectively.

In Figure 7 the $\Delta\Delta\alpha_a$(460 nm, *t*) curve is equal to α_{a,Ret_460}(460 nm, *t*) and shows the Ret_460 development with storage time *t*. The $\Delta\Delta\alpha_a$(405 nm, *t*) curve was determined by the absorption of Ret_405 with a small contribution from Ret_460. The $\Delta\Delta\alpha_a$(340 nm, *t*) curve was dominated by the absorption of Ret_340 with contributions from Ret_405 and Ret_460.

The isomerization dynamics of Ret_580_I and Ret_580_{II} and the deprotonation dynamics of the isomer products Ret_500 and Ret_460 were described by a differential equation system which was solved numerically. The involved absorption cross-sections and the time parameters were determined by fitting the calulations to the experimental results. Absorption cross-section spectra of Ret_580, Ret_500, Ret_460 and Ret_405 are shown in Figure S10 of Section S3 of the Supplementary Materials. The Ret_580 decay time development is presented in Figure S11 of Section S4 of the Supplementary Materials. It is thought that it was caused by structural changes of the QuasAr1 apoprotein with storage time.

The fit of calculated curves to the experimental data in Figures 6 and 7 is reasonably good. Only the numerical curve $\Delta\Delta\alpha_a$(λ = 340 nm, *t*) does not fit well to the experimental points, indicating additional minor isomerization and deprotonation paths of the originally present (Ret_580_I, Ret_580_{II}) and formed (Ret_500; Ret:460) constituents of QuasAr1 which are not included the model.

6. Conclusions

The previously invested absorption spectroscopic thermal dynamics of the Archaerhodopsin 3 based fluorescent voltage sensor QuasAr1 [17] was reanalyzed in detail and was numerically simulated with a differental equation system. The combined experimemtal and theoretical investigation allows model developments and avoids misinterpretations. This makes it possible to calculate quantitative reaction paramters.

The absorption spectroscopic studies performed at room temperature in the dark enable us to evaluate the thermal stability of the sample under investigation; this is a prerequiste to carrying out purpose applications of interest, such as the investigation of the photocycle dynamics of QuasAr1 [28]. The presented findings indicate that QuasAr1 can be used for approximately 10 h in its initial form before the onset of modifications due to aggregation and ground-state isomerization.

The thermal dynamics results obtained here for QuasAr1 cannot be used to estimate the thermal behavior of other variants of Archaerhodopsin 3 based voltage sensors, as is shown by the results obtained for Archon2 [29] (there was no indication of protonated retinal Schiff base ground-state isomerization and there was an onset of light scattering after

two days due to beginning of protein unfolding). The thermal stability of each microbial rhodopsin based voltage sensor needs to be investigated individually.

Supplementary Materials: The following supporting information can be downloaded at: https://www.mdpi.com/article/10.3390/bioengineering12121293/s1, Figure S1: Temporal development of attenuation coefficient spectra of QuasAr1 in pH 8 Tris buffer at room temperature in the dark; Figure S2: Temporal development of absorption coefficient spectra of QuasAr1 in pH 8 Tris buffer at room temperature in the dark; Figure S3: Temporal development of absorption coefficients at wavelengths 580 nm, 500 nm, 460 nm, 405 nm, and 340 nm of QuasAr1 in pH 8 Tris buffer at room temperature in the dark; Figure S4: Temporal development of absorption coefficient difference spectra of QuasAr1 in pH 8 Tris buffer at room temperature in the dark; Figure S5: Temporal development of absorption coefficient double difference spectra of QuasAr1 in pH 8 Tris buffer at room temperature in the dark; Figure S6: Scattering cross-section at 750 nm versus storage time for QuasAr1 in pH 8 Tris buffer at room temperature in the dark; Figure S7: Temporal development of aggregation scattering enhancement factor; Figure S8: Calculated scattering coefficient spectra of QuasAr1 in pH 8 Tris buffer at room temperature in the dark for various storage times; Figure S9: Variation of adjusted Mie scattering power factor with storage time for sample of QuasAr1 in pH 8 Tris buffer at room temperature in the dark; Figure S10: Absorption cross-section spectra of Ret_580, Ret_500, Ret_460 and Ret_405; Figure S11: Temporal development of time constants of isomerization of Ret_580$_{I}$ and Ret_580$_{II}$; Table S1: Scattering relevant parameters of Quasar1 at 750 nm; Table S2: Amino acid numbers, molar refractivity values, volume densities, and molar masses of constituents of QuasAr1. References [30–38] are cited in the Supplementary Materials.

Author Contributions: The study was initiated by A.S. and P.H. The calculations were carried out by A.P. The manuscript was written by A.P. and commented and improved by A.S. and P.H. All authors have read and agreed to the published version of the manuscript.

Funding: This research received no external funding.

Data Availability Statement: The original contributions presented in this study are included in the article/Supplementary Material. Further inqueries can be directed to the corresponding author.

Acknowledgments: Alfons Penzkofer thanks Franz J. Gießibl, University of Regensburg, for his kind hospitality. Peter Hegemann thanks the Hertie-Foundation for awarding and support.

Conflicts of Interest: The authors declare no conflict of interest.

Abbreviations

Arch	Archaerhodopsin 3 from *Halorubrum sodmense*
GEVI	Genetically encoded voltage indicator
PRSB	Protonated retinal Schiff base
QuasAr	Quality superior to Arch
Ret_xxx	Retinal with absorption maximum approximately at xxx nm
RSB	Retinal Schiff base

Symbols

Parameter	**Unit**	**Meaning**
a_{ag}	nm	Aggregate radius
a_m	nm	Monomer radius
$\widetilde{M}$		Total Mie scattering function
M_m	g mol^{-1}	Molar mass
M_{sca}		Aggregation scattering enhancement factor
N_0	cm^{-3}	QuasAr1 number density
$N_{Ret\_580,0}$	cm^{-3}	Initial number density of Ret_580 at t = 0
$N_{Ret\_580,I}$	cm^{-3}	Number density of Ret_580$_{I}$
$N_{Ret\_580,II}$	cm^{-3}	Number density of Ret_580$_{II}$

N_{Ret_xxx}	cm^{-3}	Number density of Ret_xxx
n_w		Refractive index of water (solvent)
n_Q		Refractive index of QuasAr1 (solute)
t	h	Storage time
α	cm^{-1}	Attenuation coefficient
α_a	cm^{-1}	Absorption coefficient
α_s	cm^{-1}	Scattering coefficient
$\Delta\alpha_a$	cm^{-1}	Absorption coefficient difference
$\Delta\Delta\alpha_a$	cm^{-1}	Absorption coefficient double difference
β_m		Degree of aggregation
γ		Mie scattering power factor
κ_I		Initial fraction of Ret_580_I in Ret_580
κ_{II}		Initial fraction of Ret_580_{II} in Ret_580
λ	nm	Vacuum wavelength
σ_a	cm^2	Absorption cross-section
$\sigma_{R,ag}$	cm^2	Rayleigh aggregate scattering cross-section
$\sigma_{R,m}$	cm^2	Rayleigh monomer scattering cross-section
σ_s	cm^2	Scattering cross-section
$\tau_{Ret\_580_I}$	h	Isomerization time constant of Ret_580_I
$\tau_{Ret\_580_{II}}$	h	Isomerization time constant of Ret_580_{II}
τ_{Ret_500}	h	Deprotonation time constant of Ret_500
τ_{Ret_460}	h	Deprotonation time constant of Ret_460

References

1. Ihara, K.; Umemura, T.; Katagirri, I.; Kitajima-Ihara, T.; Sugiyama, Y.; Kimura, Y.; Mukohata, Y. Evolution of archaeal rhodopsins: Evolution rate changes by gene duplication and functional differentiation. *J. Mol. Biol.* **1999**, *285*, 163–174. [CrossRef]
2. Kralj, J.M.; Douglass, A.D.; Hochbaum, D.R.; Maclaurin, D.; Cohen, A.E. Optical recording of action potentials in mammalian neurons using a microbial rhodopsin. *Nat. Methods* **2012**, *9*, 90–95. [CrossRef]
3. Herasymenko, K.; Walisinghe, D.; Konno, M.; Barneschi, L.; de Waele, I.; Sliwa, M.; Inoue, K.; Olivucci, M.; Haacke, S. Archaerhodopsin 3 is an ideal template for the engineering of highly fluorescent optogenetic reporters. *Chem. Sci.* **2024**, *16*, 761–774. [CrossRef]
4. Hochbaum, D.R.; Zhao, Y.; Farhi, S.L.; Klapoetke, N.; Werley, C.A.; Kapoor, V.; Zou, P.; Kralj, J.M.; Maclaurin, D.; Smedemark-Margulies, N.; et al. All-optical electrophysiology in mammalian neurons using engineered microbial rhodopsins. *Nat. Methods* **2014**, *11*, 825–833. [CrossRef]
5. St-Pierre, F.; Chavarha, M.; Lin, M.Z. Designs and sensing mechanisms of genetically encoded fluorescent voltage indicators. *Curr. Opin. Chem. Biol.* **2015**, *27*, 31–38. [CrossRef]
6. Platisa, J.; Pieribone, V.A. Genetically encoded fluorescent voltage indicators: Are we here yet? *Curr. Opin. Neurobiol.* **2018**, *50*, 146–153. [CrossRef]
7. Haider, T.A.; Knöpfel, T. Voltage-sensitive fluorescent proteins for optical electrophysiology. In *Neural Interface Engineering*; Guo, L., Ed.; Springer Nature: Cham, Switzerland, 2000; pp. 383–407.
8. Mollinedo-Gajate, I.; Song, C.; Knöpfel, T. Genetically encoded voltage indicators. *Adv. Exp. Med. Biol.* **2021**, *1293*, 209–224. [CrossRef] [PubMed]
9. Zhang, X.M.; Yokoyama, T.; Sakamoto, M. Imaging voltage with microbial rhodopsin. *Front. Mol. Biosci.* **2021**, *8*, 738829. [CrossRef] [PubMed]
10. Silapetere, A.; Hwang, S.; Hontani, Y.; Lahore, R.G.F.; Balke, J.; Escobar, F.V.; Tros, M.; Konold, P.E.; Matis, R.; Croce, R.; et al. QuasAr odyssey: The origin of fluorescence and its voltage sensitivity in microbial rhodopsins. *Nat. Commun.* **2022**, *13*, 5501. [CrossRef] [PubMed]
11. Meng, X.; Ganapathy, S.; van Roemburg, L.; Brinks, D. Voltage imaging with engineered proton-pumping rhodopsins: Insights from the proton transfer pathway. *ACS Phys. Chem. Au* **2023**, *3*, 320–333. [CrossRef]
12. Sakamoto, M.; Yokoyama, T. Probing neuronal activity with genetically encoded calcium and voltage fluorescent indicators. *Neurosci. Res.* **2025**, *215*, 56–63. [CrossRef]
13. Peterka, D.S.; Takahashi, H.; Yuste, R. Imaging voltage in neurons. *Neuron* **2011**, *69*, 9–21. [CrossRef]
14. Rettinger, J.; Schwarz, S.; Schwarz, J. *Electrophysiology. Basics, Methods, Modern Approaches and Applications*, 2nd ed.; Springer Nature: Cham, Switzerland, 2022.

15. Mei, G.; Mamaeva, N.; Ganapathy, S.; Wang, P.; DeGrip, W.J.; Rothschild, K.J. Analog retinal redshifts visible absorption of Quasar transmembrane voltage sensors into near-infrared. *Photochem. Photobiol.* **2020**, *96*, 55–66. [CrossRef]
16. Streit, J.; Kleinlogel, S. Dynamic all-optical drug screening on cardiac voltage-gated ion channels. *Sci. Rep.* **2018**, *8*, 1153. [CrossRef]
17. Penzkofer, A.; Silapetere, A.; Hegemann, P. Absorption and emission spectroscopic investigation of the thermal dynamics of the Archaerhodopsin 3 based fluorescent voltage sensor QuasAr1. *Int. J. Mol. Sci.* **2019**, *20*, 4086. [CrossRef] [PubMed]
18. Van de Hulst, H.C. *Light Scattering by Small Particles*; John Wiley and Sons: New York, NY, USA, 1957.
19. Kerker, M. *The Scattering of Light and other Electromagnetic Radiation*; Academic Press: New York, NY, USA, 1969.
20. Gratz, H.; Penzkofer, A.; Weidner, P. Nanometer particle size, pore size, and specific surface determination of colloidal suspensions and porous glasses by Rayleigh light scattering. *J. Non Cryst. Solids* **1995**, *189*, 50–54. [CrossRef]
21. Bohren, G.F.; Huffman, D.R. *Absorption and Scattering of Light by Small Particles*; John Wiley and Sons: New York, NY, USA, 1983.
22. Brown, W. (Ed.) *Light Scattering Principles and Development*; Clarendon Press: Oxford, UK, 1996.
23. Weigand, R.; Rotemund, F.; Penzkofer, A. Degree of aggregation of indocyanine green in aqueous solutions determined by Mie scattering. *Chem. Phys.* **1997**, *220*, 373–384. [CrossRef]
24. Penzkofer, A.; Shirdel, J.; Zirak, P.; Breitkreuz, H.; Wolf, E. Protein aggregation studied by forward light scattering and light transmission analysis. *Chem. Phys.* **2007**, *342*, 55–63. [CrossRef]
25. Hergert, W.; Wriedt, T. (Eds.) *The Mie Theory: Basics and Applications*; Springer: Berlin/Heidelberg, Germany, 2012.
26. Jagger, J. *Introduction to Research in Ultraviolet Photobiology*; Prentice Hall: Englewood Cliffs, NJ, USA, 1967.
27. Oster, G. Light scattering. In *Physical Techniques in Biological Research*; Oster, G., Pollister, A.W., Eds.; Academic Press: New York, NY, USA, 1955; Volume 1, p. 51.
28. Penzkofer, A.; Silapetere, A.; Hegemann, P. Photocycle dynamics of the Archaerhodopsin 3 based fluorescent voltage sensor QuasAr1. *Int. J. Mol. Sci.* **2020**, *21*, 160. [CrossRef]
29. Penzkofer, A.; Silapetere, A.; Hegemann, P. Absorption and emission spectroscopic investigation of the thermodynamics of the Archaerhodopsin 3 based fluorescent voltage sensor Archon2. *Int. J. Mol. Sci.* **2020**, *21*, 6576. [CrossRef] [PubMed]
30. Jenkins, F.A.; White, H.E. *Fundamentals of Optics*, 3rd ed.; McGraw-Hill: Tokyo, Japan, 1957.
31. Pankove, J.I. *Optical Processes in Semiconductors*; Dover Publications: New York, NY, USA, 1971.
32. Hale, G.M.; Querry, M.R. Optical constants of water in the 200-nm to 200-µm wavelength region. *Appl. Opt.* **1973**, *12*, 555–563. [CrossRef]
33. Fischer, H.; Polikarpov, I.; Craievich, A. Average protein density is a molecular-weight-dependent function. *Protein Sci.* **2004**, *13*, 2825–2828. [CrossRef]
34. Atkins, P.W. *Physical Chemistry*, 2nd ed.; Oxford University Press: Oxford, UK, 1992; pp. 772–778.
35. McMeekin, T.L.; Wilensky, M.; Groves, M.L. Refractive indices of proteins in relation to amino acid composition and specific volume. *Biochem. Biophys. Res. Commun.* **1962**, *7*, 151–156. [CrossRef]
36. Zhao, H.; Brown, P.H.; Schuck, P. On the distribution of protein refractive index increments. *Biophys. J.* **2011**, *100*, 2309–2327. [CrossRef] [PubMed]
37. De Melo Sales, T.R.; de Melo, C.P. Charge transfer versus isomerization effects on the polarizabilities of retinal analogs. *Chem. Phys. Lett.* **1991**, *180*, 105–108. [CrossRef]
38. Toto, J.L.; Toto, T.T.; de Melo, C.P.; Robins, K.A. *Ab initio* studies of the polarizabilities of retinal analogs. *J. Phys. Chem.* **1994**, *101*, 3945–3951. [CrossRef]